PCCP

Photodissociation dynamics of carbonyl chloride fluoride and its implications for phosgene three body decay

Christof Maul,[a] Christoph Dietrich,[b] Tobias Haas[c] and Karl-Heinz Gericke[a]

[a] *Institut für Physikalische und Theoretische Chemie, Technische Universität Braunschweig, Hans-Sommer-Str. 10, 38106 Braunschweig, Germany. E-mail: c.maul@tu-bs.de; Fax: +49 531 3915396*
[b] *Merck, Frankfurter Str. 250, 64293 Darmstadt, Germany*
[c] *Linopress, Frankfurter Str. 21-25, 65760 Eschborn, Germany*

Received 7th December 1998, Accepted 4th February 1999

The photodissociation dynamics of COFCl has been studied by monitoring Cl fragments by resonance enhanced multi-photon ionisation and time-of-flight techniques at dissociation wavelengths near 235 nm. The COFCl heat of formation and the dissociation energy for C—Cl bond fission were for the first time experimentally determined: $\Delta_f H_0^0$ (COFCl) = -397 ± 15 kJ mol^{-1} and D_0(COF—Cl) = 364 ± 8 kJ mol^{-1}. 35% of the available energy is channelled into FCO rotation and bending vibration. The remaining energy is released as product translation. Other than in phosgene, no spin–orbit state selective behaviour is observed. The observations agree with a decay mechanism within the COFCl molecular plane as well as with a fragmentation *via* out-of-plane movement of the departing Cl atom. The structural and electronic similarity of COFCl and $COCl_2$ allows conclusions to be drawn on the $COCl_2$ dissociation. The findings are evidence for a previously proposed decay mechanism for the asynchronous concerted three body decay of phosgene into CO + 2Cl. The first bond cleavage produces ground and excited spin–orbit state Cl and Cl*, respectively, with large kinetic energy release, while breaking the second C—Cl bond exclusively generates slow ground state Cl atoms.

1 Introduction

The chemistry of carbonyl halides has found wide attraction for the use of phosgene in the chemical industry, namely as an intermediate in the polyurethane production and as a reagent in the synthesis of pharmaceuticals, and has comprehensively been reviewed only recently.[1] However, photolysis studies are less abundant, especially for compounds other than phosgene, although they are of interest for a number of reasons.

First, the role of carbonyl halides in atmospheric chemistry needs to be taken into account. Phosgene ($COCl_2$),[2] carbonyl chloride fluoride (COFCl),[3] and carbonyl fluoride (COF_2)[4] have been detected in the stratosphere and, with the exception of COFCl, in the troposphere as well, and significant concentration increases have been observed.[4] $COCl_2$ and COFCl are mainly photolytically or chemically produced from fully or partially halogenated chloro(fluoro)carbon precursor molecules (CFCs and HCFCs).[5–7] Tropospheric carbonyl halides are essentially unreactive because they will primarily be removed by heterogeneous decomposition through contact with surfaces and liquid phase hydrolysis, particularly within clouds.[6,7] In the stratosphere, however, photolysis becomes the major removal pathway besides transport into the troposphere, and the released chlorine can participate in the catalytic destruction of ozone.[7]

Second, carbonyl halides serve as an easily accessible prototype for the study of an up to date only scarcely investigated chemical elementary process: the photo-induced decomposition of a molecule into three fragments, ABC + $h\nu \rightarrow$ A + B + C.[8] What makes carbonyl halides unique in this respect, is the production of easily detectable fragments such as chlorine atoms upon irradiation in an easily accessible ultraviolet (UV) wavelength range.

In order to be able to both evaluate the atmospheric significance of the carbonyl halide photolysis and to assess the dynamics of a three body fragmentation process, the primary photolytic decay channels as well as the thermochemical properties of the parent molecules and the dissociation fragments have to be accurately known. Whereas for the well-characterised phosgene molecule corresponding studies could directly be performed based on the knowledge of the respective quantities,[9,10] for COFCl only calculated or estimated literature values exist for the heat of formation $\Delta_f H^0$ and for the dissociation energy D_0,[1,11] which have still to be verified experimentally. Therefore, in this work we investigated the energetics as well as the dynamics of the photodissociation of COFCl at a wavelength of 235 nm.

Due to significant uncertainties of the reported thermochemical data for the carbonyl compounds[11] relevant to this work, several product channels might be open at this wavelength:

$$\mathrm{COFCl} + h\nu \rightarrow \mathrm{COF} + \mathrm{Cl} \quad (1)$$

$$\mathrm{CO} + \mathrm{F} + \mathrm{Cl} \quad (2)$$

$$\mathrm{COCl} + \mathrm{F} \quad (3)$$

$$\mathrm{CO} + \mathrm{FCl} \quad (4)$$

More reliable reaction enthalpies and threshold wavelengths will be obtained from the data presented in this work. Previously, upon photodissociation between 193 and 248 nm, channels (1)–(3) were found to operate in competition.[12,13] At 235 nm, however, for Cl production, channel (1) is expected to be dominating, because for channel (2) the photon energy is only slightly above threshold. Moreover, channels (3) and (4) can only contribute to the Cl yield *via* secondary photolysis of

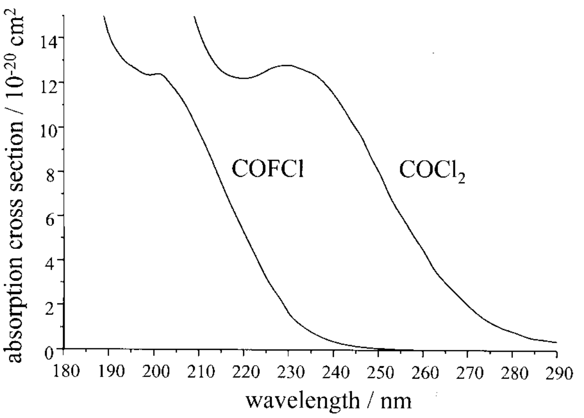

Fig. 1 Absorption spectra of COFCl and of $COCl_2$. The first absorption bands, corresponding to a $\pi^* \leftarrow n$ transition, are almost identical, except for being shifted by *ca.* 30 nm.

primary COCl or FCl products and can therefore easily be recognised and distinguished from channel (1) from their energetics.

The investigation of the COFCl photodissociation will facilitate the understanding of the previously investigated three body decay of phosgene, where a competition between synchronous one-step and non-synchronous two-step fragmentation into CO + 2Cl has been found to take place.[9,10] The partial fluorination of phosgene inhibits the three body channel for COFCl dissociation by stabilising the FCO intermediate and simplifies the dissociation. At the same time, the similarity of COFCl and $COCl_2$ allows the results of the photolysis studies for both molecules to be directly compared.[14] Therefore, by determining the energy partitioning into Cl + FCO fragments generated in the two body fragmentation of COFCl, one can inspect details of a single pathway in the complex three body fragmentation scheme of $COCl_2$. Thus, implications for the first step ($COCl_2 \rightarrow Cl + COCl$) of the asynchronous concerted three body decay of $COCl_2$ can be discussed from analogy considerations without disturbing interference from the second step ($COCl \rightarrow Cl + CO$) or from synchronous three body decay ($COCl_2 \rightarrow CO + 2\,Cl$).

In analogy to phosgene, ground state COFCl is a planar molecule. Its X $^1A'$ ground state electronic configuration is

$$\cdots (11a')^2(12a')^2(2a'')^2(13a')^2(14a')^2(3a'')^2(15a')^2(4a'')^2(16a')^2$$

and belongs to the C_s symmetry point group. The three highest occupied molecular orbitals are linear combinations of non-bonding n(Cl)- and n(O)-orbitals.[15] Fig. 1 demonstrates that the COFCl electronic absorption spectrum[14,16] is very similar to the phosgene absorption spectrum[17,18] except for being blue-shifted by *ca.* 30 nm due to the high F atom electronegativity.[14] It consists of a series of bands, the diffuseness of which is attributed to predissociation and which merge into a continuum at 235 nm. As in phosgene, this part of the absorption spectrum has been associated with a singlet–singlet $\pi^* \leftarrow n$ transition.[14]

2 Experimental

A detailed description of the experimental set-up of the experiment has been given elsewhere.[19] It consists of a home-built single-field time-of-flight (TOF) spectrometer with a drift region of a total length of 57 cm. The spectrometer was evacuated to a base pressure of 10^{-4} Pa (10^{-6} mbar) by a 360 l s^{-1} turbo molecular pump (Leybold Turbovac 360 CSV) and two 500 l s^{-1} oil diffusion pumps (Leybold Baur 1). Carbonyl chloride fluoride[20] was stored in a stainless steel tank, filled into a glass vessel prior to each experimental run without further purification and fed into the spectrometer *via* a supersonic jet, generated in an inductively driven pulsed nozzle (General Valve Series 9) with a diameter of 0.5 mm. The valve was operated at a stagnation pressure of typically 2×10^4 Pa (200 mbar) and a pulse duration of 250 μs, resulting in an operational background pressure of less than 10^{-3} Pa (10^{-5} mbar) at a repetition rate of 10 Hz.

Simultaneous dissociation of carbonyl chloride fluoride and state-selective detection of Cl atoms was performed using an excimer laser pumped dye laser (Lambda Physik LPD 3000/ Lambda Physik LPX 605i), operated with Coumarin-47 at a repetition rate of 10 Hz. Its output was frequency doubled by a BBO crystal and focused into the spectrometer by a 60 mm lens with a typical energy of 200 μJ per pulse. The laser beam intersected the molecular beam at an angle of 54°, while the spectrometer formed an angle of 90° with both the laser and the molecular beam axes. The particle density in the expansion zone was varied over a wide range in order to investigate space charge effects and kept well below the onset of Coulomb distortion when running experiments. Immediately after each measurement the background signal was monitored with the laser delayed with respect to the gas pulse under otherwise identical conditions and subtracted from the previously obtained TOF profile. Atomic chlorine was resonantly ionised by a (2 + 1)-REMPI scheme, employing the $4p\,^2D^0_{3/2} \leftarrow 3p\,^2P_{3/2}$ transition at 235.336 nm for ground state atoms and the $4p\,^2P^0_{1/2} \leftarrow 3p\,^2P_{1/2}$ transition at 235.205 nm for excited spin–orbit state atoms as resonance enhanced steps.[21]

Ions were detected by a double stage multi-channel plate assembly (Galileo) with an active diameter of 40 mm. After passing a discriminator (FAST 7011), the ion signal was monitored by a multi-hit time-to-digital converter (FAST 7885) with a time resolution that can be varied from 5 to 80 ns, stored in a data buffer (FAST MCD/PC), transferred to a personal computer and converted into translational energy distributions.[22] Typical acquisition times for a single TOF profile were 3000 s with a total of 3×10^5 ion counts.

The spectrometer was calibrated by monitoring kinetic energy distributions of Cl fragments from the well-characterised photodissociation of molecular Cl_2 at 308 nm.[23] The experimentally determined values are in excellent agreement with the values calculated from the spectrometer geometry. The kinetic energy resolution is energy dependent and has previously been determined to be approximately 5% for the energy values encountered.[10]

3 Results and discussion

3.1 Time-of-flight profiles

In Fig. 2 two TOF profiles are shown, where the lower trace describes the Cl($^2P_{3/2}$) electronic ground state and the upper trace the Cl*($^2P_{1/2}$) excited spin–orbit state. The structureless TOF distributions peak at t_0(Cl) = 324.8 μs and t_0(Cl*) =

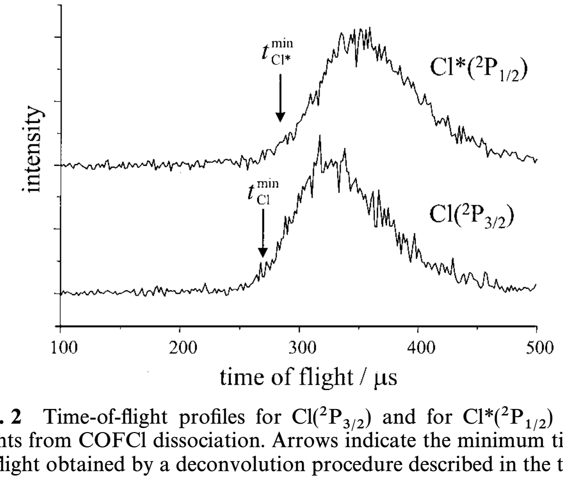

Fig. 2 Time-of-flight profiles for Cl($^2P_{3/2}$) and for Cl*($^2P_{1/2}$) fragments from COFCl dissociation. Arrows indicate the minimum times-of-flight obtained by a deconvolution procedure described in the text.

347.6 μs, respectively, and exhibit a full width at half maximum of *ca.* 100 μs. The difference in the peak position is solely due to the slightly different photolysis wavelengths (235.205 nm for Cl*, 235.338 nm for Cl) and the electronic spin–orbit energy $E_{\Omega} = 882\ \mathrm{cm}^{-1}$ of the Cl* atom.

In order to obtain the values $T_{\mathrm{Cl}}^{\max} = \frac{1}{2}m_{\mathrm{Cl}}(v_{\mathrm{Cl}}^{\max})^2$ and $T_{\mathrm{Cl*}}^{\max} = \frac{1}{2}m_{\mathrm{Cl}}(v_{\mathrm{Cl*}}^{\max})^2$ for the maximum kinetic energy release into the Cl and the Cl* fragments, one needs to determine the corresponding maximum centre of mass speed $v^{\max}$. The centre of mass speed v is obtained from the experimentally observed time of flight t by means of a centre of mass to laboratory coordinate transformation: $v = \sqrt{v_{\mathrm{beam}}^2 + s^2/t^2}$, considering the collective speed v_{beam} of the molecular beam and the spectrometer length s. Thus, the maximum centre of mass speed $v^{\max}$ relates to the minimum TOF $t^{\min}$ of the fastest fragments, the determination of which, taking into account the experimental response function and the application of an appropriate definition for $t^{\min}$, are required.

For flight times smaller than the peak position ($t \leqslant t_0$) the TOF profiles of Fig. 2 can be fitted to a very high degree of accuracy by Gaussian functions with widths $\sigma_{\mathrm{fit}}(\mathrm{Cl}) = 28.8$ μs and $\sigma_{\mathrm{fit}}(\mathrm{Cl^*}) = 32.9$ μs. Since the experimental response function has previously been determined to be of Gaussian shape with a width $\sigma_{\mathrm{resp}} = 7$ μs,[10] in order to determine $t^{\min}$ we preferred rather to deconvolute the Gaussian best fits with the known response function than to apply a forward convolution procedure.[24] Generally, the deconvolution of a Gaussian function of width σ_1 with another Gaussian function of width σ_2 again results in a Gaussian function with a width of $\sigma_{\mathrm{decon}} = \sqrt{\sigma_1^2 - \sigma_2^2}$. Thus, identifying σ_1 with σ_{fit} and σ_2 with σ_{resp}, one obtains for the deconvoluted widths σ_{decon} of the two time-of-flight profiles from Fig. 2 $\sigma_{\mathrm{decon}}(\mathrm{Cl}) = 27.9$ μs and $\sigma_{\mathrm{decon}}(\mathrm{Cl^*}) = 32.2$ μs.

For determining $t^{\min}$ the reversal point in the wing of the deconvoluted Gaussian was projected along the tangent onto the time axis. The corresponding point of intersection has a distance of $2\sigma_{\mathrm{decon}}$ from the peak position: $t^{\min} = t_0 - 2\sigma_{\mathrm{decon}}$. According to this procedure, the minimum flight times are $t_{\mathrm{Cl}}^{\min} = 269$ μs and $t_{\mathrm{Cl*}}^{\min} = 283.2$ μs for Cl and Cl*, respectively, as indicated by arrows in Fig. 2.

These values correspond to maximum velocities of $v_{\mathrm{Cl}}^{\max} = 2175\ \mathrm{ms}^{-1}$ and $v_{\mathrm{Cl*}}^{\max} = 2075\ \mathrm{ms}^{-1}$, where a molecular beam velocity $v_{\mathrm{beam}} = 500\ \mathrm{ms}^{-1}$ has been accounted for. The latter value is calculated under the reasonable assumption of complete cooling of rotational and translational degrees of freedom in the jet expansion. As a result, maximum kinetic energies of $T_{\mathrm{Cl}}^{\max} = 6980\ \mathrm{cm}^{-1}$ and $T_{\mathrm{Cl*}}^{\max} = 6340\ \mathrm{cm}^{-1}$ are obtained, where experimental uncertainties are 5%.

3.2 Fragmentation channels

In principle, atomic chlorine could be produced by a number of mechanisms: direct production in reaction (1) or in reaction (2), secondary photolysis of COCl from reaction (3), secondary photolysis of FCl from reaction (4), or two-photon dissociation of COFCl. However, in the experiments described here, only the first mechanism, direct production of Cl in reaction (1), needs to be considered, as is discussed in the following.

Coherent two-photon absorption by the COFCl parent molecule would result in available energies of 538 kJ mol^{-1} for three body decay and 654 kJ mol^{-1} for two body decay into ground state products, resulting in maximum kinetic energies of 25 780 and 31 340 cm^{-1} for atomic chlorine fragments, which are larger than the observed values by a factor of 4 and 5, respectively. The energy partitioning in the secondary photolysis of COCl or FCl has to be evaluated employing a more complex scheme. In a first step, the maximum velocity of the COCl or FCl fragment from the primary fragmentation step has to be calculated, followed by the analogous calculation of the maximum velocity of the final Cl fragment in the centre of mass system of the primary COCl or FCl fragment. Last, the respective velocities must be added up to obtain the maximum laboratory speed of the final Cl fragment. The maximum velocities of the COCl and FCl fragments from the primary fragmentation step are determined by the respective primary available energies of 99 and 276 kJ mol^{-1} and are calculated to be 850 and 1860 m s^{-1}. Secondary photolysis of COCl would transfer as much as 16 300 cm^{-1}, secondary photolysis of FCl 7700 cm^{-1} into Cl kinetic energy in the respective COCl and FCl centre of mass frames, corresponding to maximum centre of mass velocities of 3330 and 2290 m s^{-1}. Thus, the resulting maximum lab velocities of the final Cl fragments from secondary photolysis of COCl and FCl are almost identical (4180 and 4150 m s^{-1}), but much larger than the experimentally observed maximum velocity of slightly less than 2200 m s^{-1}. Again, this results in a maximum Cl kinetic energy that is larger than the observed values by almost a factor of 4. Thus, Cl production from secondary photolysis or from two-photon dissociation must be ruled out under our experimental conditions.

Three body dissociation into F + Cl + CO leaves only 29 kJ mol^{-1} to be partitioned onto the three fragments. The maximum kinetic energy for an atomic chlorine fragment is determined by the mass ratio $m_{\mathrm{FCO}}/m_{\mathrm{COFCl}} = 47/82$ and amounts to 16.6 kJ mol^{-1}, corresponding to a maximum fragment velocity in the COFCl centre of mass frame of 970 m s^{-1}. Taking into account the molecular beam velocity of 500 m s^{-1}, the maximum lab velocity amounts to 830 m s^{-1}, corresponding to a minimum TOF of 680 μs in the 57 cm drift tube. While the contribution of three body decay cannot be ruled out by energetic reasons, the time domain monitored in the experiment ($0 \leqslant t \leqslant 640$ μs) does not contain fragments from three body dissociation.

Thus, the TOF profiles shown in Fig. 2 exclusively result from channel (1): two body dissociation into COF + Cl induced by COFCl one-photon absorption in the first absorption band.

3.3 Dissociation energy D_0(COF—Cl)

The dissociation energy D_0(COF—Cl) can be determined from evaluating the energy balance for process (1):

$$\begin{aligned} E_{\mathrm{av}} &= h\nu - D_0(\mathrm{COF{-}Cl}) + E_{\mathrm{COFCl}} \\ &= T_{\mathrm{FCO}} + E_{\mathrm{FCO}} + T_{\mathrm{Cl}} + E_{\mathrm{Cl}} \qquad (5) \end{aligned}$$

where the available energy E_{av} consists of the kinetic energies T and the internal energies E of both FCO and Cl fragments and is given by the sum of the photon energy $h\nu$ and the internal energy E_{COFCl} of the parent molecule, diminished by D_0. The contribution of E_{COFCl} is insignificant, as was proven by measurements of the rotational temperature of CO impurities in the supersonic beam sample which resulted in values well below 10 K. The kinetic energies T_{Cl} and T_{FCO} of the Cl and the FCO fragments are related *via* the conservation of linear momentum:

$$T_{\mathrm{FCO}} = \frac{m_{\mathrm{Cl}}}{m_{\mathrm{FCO}}} T_{\mathrm{Cl}} = \tfrac{35}{47} T_{\mathrm{Cl}} \qquad (6)$$

where m_{Cl} and m_{FCO} are the fragment masses and the minor contribution of the $^{37}\mathrm{Cl}$ isotope has been neglected. If it is assumed that for maximum total kinetic energy release $T^{\max} = T_{\mathrm{Cl}}^{\max} + T_{\mathrm{FCO}}^{\max}$ no internal energy is transferred into the FCO product, *i.e.* $E_{\mathrm{FCO}}(T^{\max}) = 0$, then for ground state Cl ($E_{\mathrm{Cl}} = 0$) eqn. (5) can be rewritten to yield:

$$D_0(\mathrm{COF{-}Cl}) = h\nu - T^{\max} = h\nu - T_{\mathrm{Cl}}^{\max}(1 + \tfrac{35}{47}) \qquad (7)$$

In the case of electronically excited Cl* the right hand side of eqn. (7) has further to be diminished by $E_{\mathrm{Cl*}} = E_{\Omega}$. Thus, the

Table 1 Heats of formation

	$\Delta_f H_0^0$/kJ mol^{-1}	Ref.
COFCl	-397 ± 15	This work
$COCl_2$	-218.4 ± 3.3	11
COF	-152.7 ± 12	25
COCl	-64 ± 42	11
CO	-113.8 ± 0.2	11
FCl	50.2 ± 0.4	11
F	77.3 ± 0.3	11
Cl	119.6	11

dissociation energy D_0(COF—Cl) can be determined by a measurement of the maximum kinetic energy release T_{Cl}^{max} (or $T_{Cl^*}^{max}$) into the Cl (or Cl*) fragment. Using eqn. (7), considering the experimental uncertainty of 5%, and taking into account the spin–orbit energy E_Ω of Cl*, the mean value for the dissociation energy D_0(COF—Cl) is $30\,450 \pm 600$ cm^{-1} = 364 ± 8 kJ mol^{-1}, calculated from the maximum kinetic energies $T_{Cl}^{max} = 6980$ cm^{-1} and $T_{Cl^*}^{max} = 6340$ cm^{-1}. Correspondingly, the available energy $E_{av} = h\nu - D_0$(COF—Cl), which must be distributed onto the various degrees of freedom of both fragments, is calculated to be $E_{av} = 12\,050 \pm 600$ cm^{-1}.

3.4 Heat of formation $\Delta_f H_0^0$(COFCl)

The COFCl heat of formation at 0 K is calculated from the above determined dissociation energy D_0(COF—Cl) and from the heats of formation of the products FCO and Cl

$$\Delta_f H_0^0(\mathrm{COFCl}) = \Delta_f H_0^0(\mathrm{Cl}) + \Delta_f H_0^0(\mathrm{FCO}) - D_0(\mathrm{COF{-}Cl}) \tag{8}$$

With the values $\Delta_f H_0^0$(FCO) = -152.7 ± 12 kJ mol^{-1} [25] and $\Delta_f H_0^0$(Cl) = 119.6 kJ mol^{-1} [11] one obtains a COFCl heat of formation of $\Delta_f H_0^0$(COFCl) = -397 ± 15 kJ mol^{-1}.

To our knowledge, this is the first experimental value for the COFCl heat of formation. It lies in between the value of -424.3 ± 33 kJ mol^{-1}, estimated from averaging over the respective COF_2 and $COCl_2$ data,[11] and a calculated value of -387 kJ mol^{-1}.[26] The value strongly depends on the FCO heat of formation, which in recent experiments[25,27] was re-evaluated to be almost 20 kJ mol^{-1} larger than the previously recommended value of -172.1 kJ mol^{-1}.[11] Despite good experimental accuracy of the re-evaluated number, some uncertainty remains with respect to the correct value of the FCO heat of formation, as is evident from recent theoretical work in which significantly smaller values were calculated.[28,29] Nevertheless, a recent study on the dissociation of HFCO[30] strongly supports the experimental value from ref. 25.

The thermochemical values used in the data analysis and determined in this work are listed in Table 1. The corresponding reaction enthalpies and threshold wavelengths for reactions (1)–(4) are compiled in Table 2 and illustrated in Fig. 3.

3.5 Energy partitioning

In Fig. 4 the TOF profiles of Fig. 2 were converted into distributions of fragment kinetic energies, taking into account the laboratory to centre-of-mass transformation, but neglecting the small contribution of the ^{37}Cl isotope.[22] The distributions appear structureless and identical to each other, apart from being shifted in energy by approximately the equivalent of the electronic spin–orbit excitation E_Ω. This identical behaviour for the two spin–orbit components is remarkable in that it strongly contrasts findings from phosgene dissociation above the three body threshold, where a pronounced spin–orbit state selectivity has been observed.[10] If the kinetic energies of both the Cl (or Cl*) and the FCO fragments, augmented by the spin–orbit energy E_Ω, where required, are subtracted from the available energy, one obtains the distribution of the FCO internal energy, as shown in Fig. 5 together with the available energy $E_{av} = h\nu - D_0$(COF—Cl). The FCO internal energy must be rotational or vibrational in nature, since the available energy is insufficient to electronically excite FCO.[31–33] The FCO internal energy peaks at 4350 cm^{-1} and is almost symmetrically distributed with a full width at half maximum of 3500 cm^{-1}. Consequently, the mean FCO internal energy $\bar{E}_{FCO}$ amounts to 4350 cm^{-1}. Thus, a fairly large amount of $f_{int} = 35\%$ of the available energy is transferred into internal energy of the FCO fragment, while the remaining portion $f_{kin} = 65\%$ appears as total kinetic energy in both fragments. An upper limit of 2% was estimated for electronic excitation of Cl. The energy partitioning data are compiled in Table 3.

Table 2 Reaction enthalpies and threshold wavelengths

Products	$\Delta_r H_0^0$/kJ mol^{-1}	λ_{thr}/nm
COF + Cl	364 ± 8^a	329
CO + F + Cl	$480 \pm 15^{a,b}$	249
COCl + F	$410 \pm 45^{a,b}$	292
CO + FCl	$233 \pm 15^{a,b}$	513

[a] This work. [b] Product heats of formation from ref. 11.

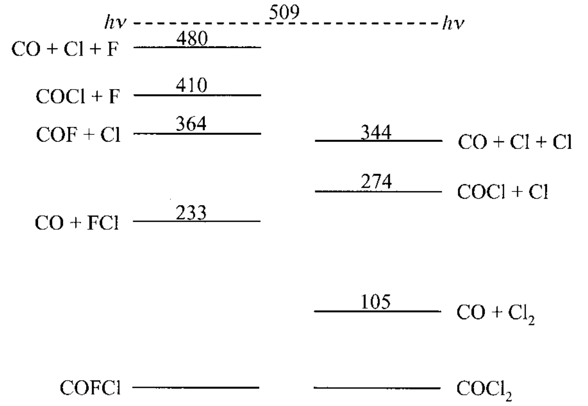

Fig. 3 Energetics for COFCl and $COCl_2$ dissociation: asymptotic product energies, given in kJ mol^{-1} relative to the respective ground state parent molecules. Thermochemical values are taken from Table 1. The dashed line indicates the photon energy $h\nu$.

The excitation of CO stretch ($\nu_1 = 1861.4$ cm^{-1}) or CF stretch ($\nu_2 = 1026.1$ cm^{-1})[34] quanta in the FCO fragment would be resolved in view of the experimental resolution of 600 cm^{-1}. The lack of any structure in the internal energy distribution of FCO suggests significant excitation of rotation ($A = 6.3778$ cm^{-1}, $B = 0.382$ cm^{-1}, $C = 0.36$ cm^{-1})[34] and

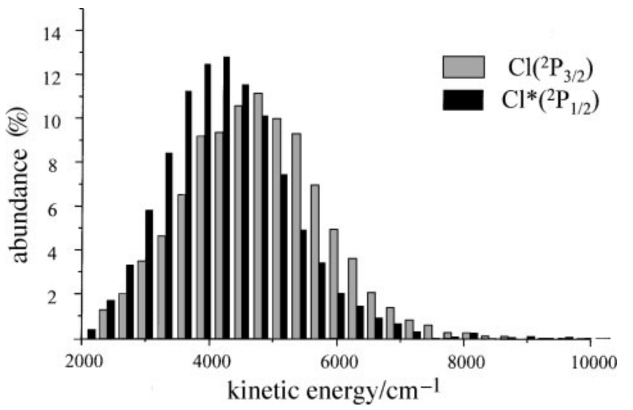

Fig. 4 Centre-of-mass fragment kinetic energy distributions derived from the time-of-flight profiles from Fig. 2. Abundances are calculated for kinetic energy intervals of 300 cm^{-1}.

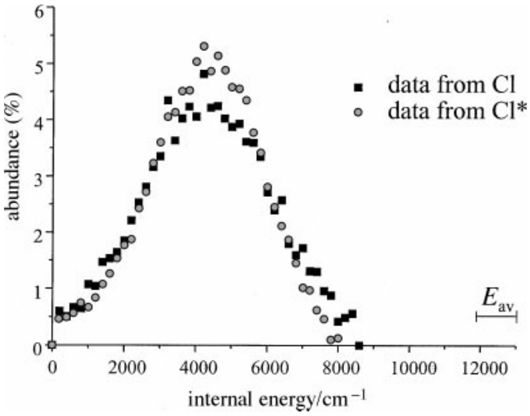

Fig. 5 FCO internal energy distribution, derived from data for ground state (black squares) and excited state (grey circles) Cl. Abundances are calculated for kinetic energy intervals of 200 cm^{-1}. The available energy indicator displays the experimental uncertainty. The unstructured internal energy distribution suggests the excitation of rotation and bending vibration only.

bending vibration ($\nu_3 = 627.5$ cm^{-1})[35] only, for which progressions cannot be resolved.

This behaviour is easily understood if the bond lengths r_{C-F} and $r_{C=O}$ and the FCO bond angle for the COFCl parent[36] and the FCO fragment[34] molecule are compared, which are compiled in Table 4. Only the FCO bond angle deviates slightly from the value in the parent while the bond lengths are almost identical. Thus, no significant dynamic excitation of the CO or the CF stretch coordinates in the FCO fragment is expected. If the parent decays from the planar ground state geometry, then the departing Cl atom should indeed induce a strong bending vibration in the fragment. If, however, COFCl decays from a bent electronically excited state or from a highly vibrationally excited ground state following internal conversion, a significant rotational excitation about the minor axis can be expected. The mean internal energy of FCO $\bar{E}_{FCO}$ is equivalent to approximately $J_m = 26$ quanta of rotation about the minor axis. Relating the mean FCO rotational angular momentum $J_m \hbar$ to the Cl—FCO orbital angular momentum $\mu v_{rel} b$ yields an impact parameter of $b = J_m \hbar/(\mu v_{rel}) \approx 25$ pm with respect to the FCO centre of mass for a departing Cl atom with mean kinetic energy $\bar{T}_{Cl}$, where μ and v_{rel} are the reduced mass and the relative velocity of the Cl—FCO system, respectively. The FCO centre of mass is calculated to lie at a distance of *ca.* 45 pm from the carbon atom, thus an impact parameter $b = 25$ pm corresponds to a mean out-of-plane angle of Cl with the FCO plane of *ca.* 35°. Both models, as simple as they are, agree with the experimental observations. Therefore, with the present data, it is not possible to decide which mechanism governs the COFCl fragmentation, although from analogy considerations with respect to the phosgene dissociation the out-of-plane mechanism is the more probable one.

Table 3 Energy partitioning

E_{av}/cm^{-1}	$\bar{E}_{FCO}$/cm^{-1}	$\bar{T}_{FCO}$/cm^{-1}	$\bar{T}_{Cl}$/cm^{-1}	f_{int}[a]	f_{kin}[a]
12450	4350	3450	4650	0.35	0.65

[a] f_{int} and f_{kin} characterise the relative energy partitioning into internal and translational degrees of freedom.

Table 4 Structural parameters of COFCl and FCO

	COFCl[a]	FCO[b]
$r_{C=O}$/pm	117.2	116.9
r_{C-F}/pm	132.4	133.4
r_{C-Cl}/pm	173.3	
∠FCO/degrees	124.7	127.3
∠FCCl/degrees	109.2	
∠ClCO/degrees	126.1	

[a] Ref. 36. [b] Ref. 14.

3.6 Implications for phosgene three body decay

In a previous study the kinetic energy distributions (KEDs) of Cl and Cl* atoms from the 235 nm photodissociation of phosgene ($COCl_2$) were determined.[10] Bimodal, spin–orbit state selective KEDs with a fast and a slow component were observed, and an overall branching ratio P(Cl)/P(Cl*) = 5.7 was obtained. The fast component of the KEDs accounts for 25% of all Cl fragments, the slow component for the remaining 75%. The fast component exhibits a Cl*/Cl branching ratio of almost 1, while the slow component almost exclusively consists of ground state Cl($^2P_{3/2}$) fragments.

A complementary study of the CO fragments[9] originating from the same dissociation process showed that the asynchronous concerted decay mechanism

$$COCl_2 + h\nu \xrightarrow{\tau_1} COCl\dagger + Cl \xrightarrow{\tau_2} CO + Cl + Cl \tag{9}$$

($\tau_2 - \tau_1 \leqslant \tau_{rot}[COCl\dagger]$) dominates the fragmentation process, in competition with the synchronous concerted mechanism

$$COCl_2 + h\nu \rightarrow CO + Cl + Cl \tag{10}$$

Here, the intermediate COCl† fragment in mechanism (9) is excited above its dissociation threshold. From a kinematic analysis of the data it was concluded that in the main, asynchronous concerted channel (9), the final CO fragment generated in the secondary decay at time τ_2 is predominantly scattered in the forward direction with respect to the primary decay at time τ_1, in consequence yielding slow Cl fragments in the second step.[8] The synchronous concerted mechanism is associated with the fastest CO fragments observed, leaving only a small amount of kinetic energy to be distributed on the coincidently generated Cl fragments.[8] These findings agree remarkably well with the results of a statistical maximum entropy analysis procedure.[9,37] Therefore, from indirect reasoning, the first step of mechanism (9) at time τ_1 was postulated to produce Cl fragments with high kinetic energies. It was suggested that the two different bond cleavages in reaction (9) at times τ_1 and τ_2 as well as the two identical bond cleavages in reaction (10) each contribute with a characteristic branching ratio and KED to the observed overall branching ratio, spin–orbit state selectivity and bimodal KEDs.

The present study of the COFCl photodissociation yields evidence to fully adopt this view and to further clarify the details of the first and the second bond cleavage in the two-step three body decay process. As outlined in Section 3.2, under the present experimental conditions exclusively the two body channel (1) is monitored, which is the analogue to the first bond cleavage of reaction (9) at time τ_1, and any interference from the three body channel (2), which is the analogue to reaction (10), is suppressed. Clearly, the COFCl results show a strictly unimodal behaviour of the observed KEDs with large kinetic energy release and no spin–orbit state selectivity at all.

Thus, transferring these findings to the phosgene dissociation yields experimental evidence for the suggested hypothesis that in the first bond cleavage of reaction (9) at time τ_1 exclusively the fast component of the KEDs is generated. This is equally true for Cl and Cl* fragments with a P(Cl*)/P(Cl) branching ratio close to unity, in qualitative accordance with the COFCl behaviour, although no attempt was undertaken to quantitatively determine the branching ratio from reaction (1). Nevertheless, signal-to-noise considerations for the TOF profiles shown in Fig. 2 imply that Cl* and Cl signal intensities are of the same order of magnitude, which in turn also holds for the respective quantum state populations if the detection probabilities are accounted for.[38,39] The detailed fragmentation behaviour of $COCl_2$ is somewhat obscured by a presumably state specific competition between the asynchronous and synchronous concerted mechanisms (9) and (10). Monitoring CO fragments in $v = 0$, 1 only, one obtains an 80% contribution of the asynchronous concerted mechanism, while it drops to 50% when monitoring Cl fragments. The latter value must be regarded as more reliable, since monitoring Cl yields a more complete (although less detailed) picture of the dissociation process, due to CO fragments hidden in vibrationally excited ($v \geqslant 2$) states which are spectroscopically dark due to rapid predissociation.

4 Conclusion

The photodissociation of COFCl has been investigated with respect to its thermochemical properties, its dynamics, and its implications for the analogous dissociation of the phosgene molecule. The heat of formation of COFCl and the dissociation energy for C—Cl bond fission were for the first time experimentally determined: $\Delta_f H_0^0(\text{COFCl}) = -397 \pm 15$ kJ mol^{-1} and $D_0(\text{COF—Cl}) = 364 \pm 8$ kJ mol^{-1}. No dissociation channel other than $\text{COFCl} + h\nu \rightarrow \text{Cl} + \text{FCO}$ was observed. 35% of the available energy is channelled into rotation and bending vibration of the FCO fragment, the remaining energy is released as product translation. The observations agree well with either a decay mechanism within the COFCl molecular plane or a fragmentation *via* out-of-plane movement of the departing Cl atom. The COFCl dissociation mimics the first C—Cl bond cleavage in the asynchronous concerted three body fragmentation of phosgene. Accordingly, the previously observed bimodality and the spin–orbit state selectivity in the phosgene three body decay are results of the first C—Cl bond cleavage producing high kinetic energy Cl atoms in both ground and excited spin–orbit states, followed by the exclusive production of slow ground state atoms upon decay of a super-excited COCl intermediate. The results demonstrate that selected parts of a complex molecular dissociation can be studied in great detail by an appropriate chemical substitution.

5 Acknowledgements

This work was financially supported by the Deutsche Forschungsgemeinschaft. Helpful discussions with F. J. Comes, Frankfurt, and R. J. Gdanitz, Braunschweig, are gratefully acknowledged. We are indebted to H. Heydtmann, Frankfurt, and H. Willner, Hannover, for the synthesis and the supply of carbonyl chloride fluoride.

6 References

1 T. A. Ryan, C. Ryan, E. A. Seddon and K. R. Seddon, *Phosgene and Related Carbonyl Halides*, Elsevier, Amsterdam, 1996.
2 S. R. Wilson, P. J. Crutzen, G. Schuster, D. W. T. Griffith and G. Helas, *Nature*, 1988, **334**, 689.
3 S. R. Wilson, G. Schuster and G. Helas, in *Ozone in the Atmosphere*, ed. R. D. Bojkov and P. Fabian, Deepak, Hampton, 1989, pp. 302–305.
4 F. Melen, E. Mahieu, R. Zander, C. P. Rinsland, P. Demoulin, G. Roland, L. Delbouille and C. Servais, *J. Atmos. Chem.*, 1998, **29**, 119 and references therein.
5 G. Helas and S. R. Wilson, *Atmos. Environ. A*, 1992, **26**, 2975.
6 M. Kanakidou, F. J. Dentener and P. J. Crutzen, *J. Geophys. Res.*, 1995, **100**, D9, 18 871.
7 T. P. Kindler, W. L. Chameides, P. H. Wine, D. M. Cunnold, F. N. Alyea and J. A. Franklin, *J. Geophys. Res.*, 1995, **100**, D1, 1235.
8 C. Maul and K.-H. Gericke, *Int. Rev. Phys. Chem.*, 1997, **16**, 1.
9 C. Maul, T. Haas and K.-H. Gericke, *J. Phys. Chem. A*, 1997, **101**, 6619.
10 C. Maul, T. Haas, K.-H. Gericke and F. J. Comes, *J. Chem. Phys.*, 1995, **102**, 3238.
11 *NIST-JANAF Thermochemical Tables*, ed. M. W. Chase Jr., *J. Phys. Chem. Ref. Data*, 1998, monograph 9.
12 M. Hermann, A. Nölle and H. Heydtmann, *Chem. Phys. Lett.*, 1994, **226**, 559.
13 A. Nölle, C. Krumscheid and H. Heydtmann, *Chem. Phys. Lett.*, 1999, **299**, 561.
14 I. Zanon, G. Giacometti and D. Picciol, *Spectrochim. Acta*, 1961, **19**, 301.
15 P. Sherwood, E. A. Seddon, M. F. Guest, M. J. Parkington, T. A. Ryan and K. R. Seddon, *J. Chem. Soc., Dalton Trans.*, 1995, 2359.
16 A. Nölle, H. Heydtmann, R. Meller and G. K. Moortgat, *Geophys. Res. Lett.*, 1993, **20**, 707.
17 D. Gillotay, P. C. Simon and L. Dierickx, *Aeron. Acta A*, 1993, **368**, 1.
18 D. C. Moule and P. D. Foo, *J. Chem. Phys.*, 1971, **55**, 1262.
19 T. Haas, C. Maul, K.-H. Gericke and F. J. Comes, *Chem. Phys. Lett.*, 1993, **108**, 202.
20 COFCl was synthesised and supplied by H. Willner, Hannover.
21 S. Arepalli, N. Presser, R. Robie and R. Gordon, *Chem. Phys. Lett.*, 1985, **118**, 88.
22 C. Maul, *Konkurrierende Dynamik beim Dreikörperzerfall von Molekülen*, Wissenschafts-Verlag Dr. Maraun, Frankfurt, 1995.
23 Y. Matsumi, K. Tonokura and M. Kawasaki, *J. Chem. Phys.*, 1992, **97**, 1065 and references therein.
24 X. S. Zhao, PhD Thesis, University of California Berkeley, 1992.
25 T. J. Buckley, R. D. Johnson III, R. E. Huie, Z. Zhang, S. C. Kuo and R. B. Clemm, *J. Phys. Chem.*, 1995, **99**, 4879.
26 M. J. S. Dewar and H. S. Rzepa, *J. Comput. Chem.*, 1983, **4**, 158.
27 V. D. Knyazev, A. Benczura and I. R. Slagle, *J. Phys. Chem. A*, 1997, **101**, 849.
28 D. A. Dixon and D. Feller, *J. Phys. Chem. A*, 1998, **102**, 8209.
29 M. R. Zachariah, P. R. Westmoreland, D. R. Burgess Jr., W. Tsang and C. F. Melius, *J. Phys. Chem. A*, 1996, **100**, 8737.
30 C. Maul, C. Dietrich, T. Haas, K.-H. Gericke, H. Tachikawa, S. Langford, M. Kono, C. L. Reed, R. N. Dixon and M. N. R. Ashfold, to be published.
31 M. M. Maricq, J. J. Szente, Y. Su and J. S. Francisco, *J. Chem. Phys.*, 1994, **100**, 8673.
32 T. Krossner, L. Zülicke, R. Vetter, M. Perec and S. D. Peyerimhoff, *J. Chem. Phys.*, 1994, **101**, 3973.
33 T. Krossner, M. Peric, R. Vetter and S. D. Peyerimhoff, *J. Chem. Phys.*, 1994, **101**, 3981.
34 K. Nagai, C. Yamada, Y. Endo and E. Hirota, *J. Mol. Spectrosc.*, 1981, **90**, 249.
35 M. E. Jacox, *J. Mol. Spectrosc.*, 1980, **80**, 257.
36 N. Heineking, W. Jäger and M. C. L. Gerry, *J. Mol. Spectrosc.*, 1993, **158**, 69.
37 C. E. M. Strauss and P. L. Houston, *J. Phys. Chem.*, 1990, **94**, 8751.
38 Y. Matsumi, K. Tonokura, M. Kawasaki, G. Inoue, S. Satyapal and R. Bersohn, *J. Chem. Phys.*, 1992, **97**, 5261.
39 H. M. Lambert, P. J. Dagdigian and M. H. Alexander, *J. Chem. Phys.*, 1998, **108**, 4460.

Paper 8/09548E